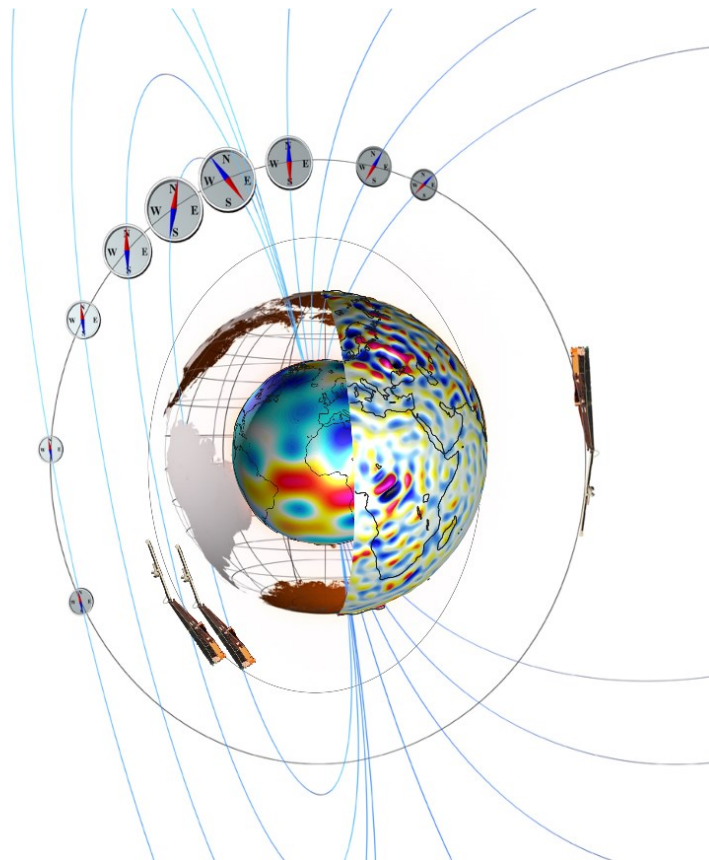

Data, Innovation, and Science Cluster

Swarm in-situ neutral horizontal winds based on Swarm plasma and neutral density measurements



Doc. no: SW-RP-DLR-GS-001, Rev: 1 dA, 06 Feb 2023

Prepared:



Timothy Kodikara

Date 06 Feb 2023

Principal Investigator

Approved:

Jens Berdermann

Date 06 Feb 2023

Commissioner Head of Institute for Solar-Terrestrial Physics
Deutsches Zentrum für Luft- und Raumfahrt (DLR), Germany

© DLR, Germany, 2023. Proprietary and intellectual rights of DLR, Germany are involved in the subject-matter of this material and all manufacturing, reproduction, use, disclosure, and sales rights pertaining to such subject-matter are expressly reserved. This material is submitted for a specific purpose as agreed in writing, and the recipient by accepting this material agrees that this material will not be used, copied, or reproduced in whole or in part nor its contents (or any part thereof) revealed in any manner or to any third party, except own staff, to meet the purpose for which it was submitted and subject to the terms of the written agreement.

Record of Changes

Reason	Description	Rev	Date
Initial vers.	Released	1 dA	06 Feb 2023

Table of Contents

1	Introduction.....	7
1.1	Scope and applicability.....	7
2	Applicable and Reference Documentation.....	7
2.1	Applicable Documents.....	7
2.2	Reference Documents.....	7
2.3	Abbreviations.....	7
3	Overview of the feasibility study.....	8
3.1	Thermosphere neutral winds.....	8
3.2	Approach.....	9
3.2.1	Lorentz terms.....	9
3.2.2	Pressure gradient.....	10
3.2.3	Ion drift velocity.....	10
3.3	Study Periods.....	10
4	Swarm-A-derived neutral horizontal winds.....	12
4.1	Comparison of the latitudinal wind patterns.....	16
4.2	Contribution from ion drift velocity.....	18
5	Summary and Conclusions.....	20
A	Lorentz terms.....	21
B	Pressure gradients.....	23
C	Nonsmoothed winds.....	25

Table of Figures

Figure 1: Swarm-A data are used in each of the input components to solve for the neutral winds in the horizontal momentum equation.	8
Figure 2: Space weather 10–14 March 2015 shown via Dst, Kp, 3-hour ap, and F10.7	11
Figure 3: Same as Figure 2 except for 19–24 September 2020.	11
Figure 4: Probability density distributions of zonal and meridional winds—2015 study period.	13
Figure 5: Same as Figure 4 except for the 2020 study period.	14
Figure 6: Statistical summary of the scalar horizontal wind speeds.	15
Figure 7: Swarm-A-derived winds compared with TIE-GCM for the 2020 study period.	16
Figure 8: Data-model differences of the scalar horizontal wind speeds.	17
Figure 9: Same as Figure 8 except for the 2020 study period.	18
Figure 10: The difference between winds derived with and without ion drift velocities.	19
Figure 11: The Pedersen ion drag coefficient ϵ_x for the 2015 study period.	21
Figure 12: Same as Figure 11 except for Hall ion drag coefficient ϵ_y	21
Figure 13: Same as Figure 11 except for the 2020 study period.	21
Figure 14: Same as Figure 12 except for the 2020 study period.	22
Figure 15: Pressure gradient Pg_X with respect to longitude—2015 study period.	23
Figure 16: Pressure gradient Pg_Y with respect to latitude—2015 study period.	23
Figure 17: Same as Figure 15 except for the 2020 study period.	23
Figure 18: Same as Figure 16 except for the 2020 study period.	24
Figure 19: Similar to Figure 5 except for nonsmoothed Swarm-A.	25

1 Introduction

This document describes the Swarm neutral horizontal winds data derived as part of the Swarm DISC Pre-study 5.1.

1.1 Scope and applicability

This document is a deliverable of the Swarm DISC Pre-study 5.1 entitled “Swarm in-situ neutral horizontal winds based on Swarm plasma and neutral density measurements” [AD-1].

This document is available on the SVN, https://smart-svn.spacecenter.dk/svn/smart/SwarmESL-All/External_Documents.

2 Applicable and Reference Documentation

2.1 Applicable Documents

The following documents are applicable to the definitions within this document.

[AD-1] SW-SW-DTU-GS-005, rev 1, Statement of Work

2.2 Reference Documents

The following documents contain supporting and background information to be considered during the activities specified within this document.

[RD-1] Kelley, M. C. (1989), Fundamentals of ionospheric plasma dynamics, in *The Earth's Ionosphere: Plasma Physics and Electrodynamics*, pp. 23– 63, Academic Press, Calif.

[RD-2] Forootan, E., Kosary, M., Farzaneh, S. et al. Forecasting global and multi-level thermospheric neutral density and ionospheric electron content by tuning models against satellite-based accelerometer measurements. *Sci Rep* 12, 2095 (2022). <https://doi.org/10.1038/s41598-022-05952-y>

[RD-3] Kodikara, T., Borries, C., Forootan, E., Doornbos, E., & Siemes, C. (2022). Swarm in-situ neutral horizontal winds based on Swarm plasma and neutral density measurements. In *Fall Meeting 2022*. AGU

2.3 Abbreviations

A list of acronyms and abbreviations used by Swarm partners can be found [here](#). Any acronyms or abbreviations not found on the online list but used in this document can be found below.

Acronym <i>or abbreviation</i>	Description
TIE-GCM	thermosphere-ionosphere-electrodynamics general circulation model
HWM	horizontal wind model
NRLMSISE-00	Naval Research Laboratory mass spectrometer and incoherent scatter radar extended-00

3 Overview of the feasibility study

The primary task of this feasibility study is to develop a prototype neutral horizontal wind product using existing Swarm data products. The neutral horizontal wind product will include both meridional (north-south) and zonal (east-west) components. The original idea proposal recognized the opportunity to create a unique data product that could be used to study, inter alia, the close coupling between the neutral winds and the ionosphere-thermosphere structure.

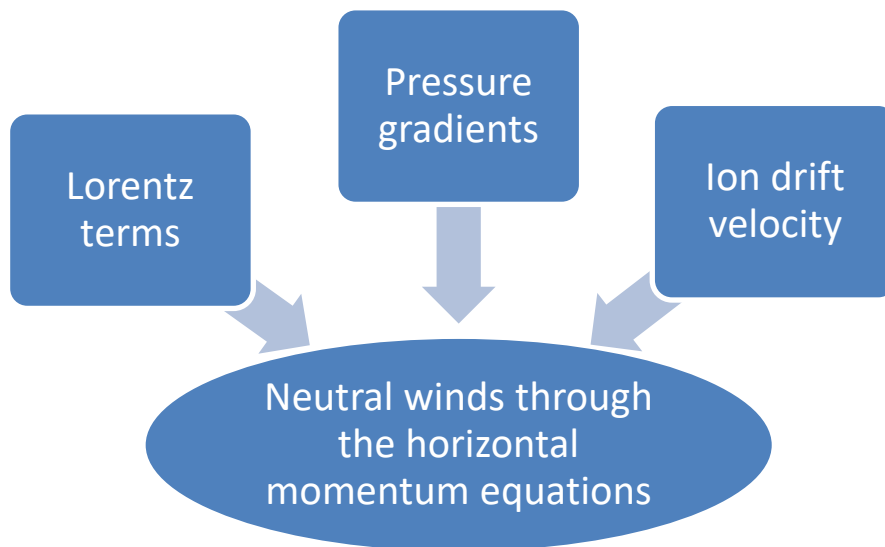


Figure 1: Swarm-A data are used in each of the input components to solve for the neutral winds in the horizontal momentum equation.

3.1 Thermosphere neutral winds

Neutral winds are key to understanding thermosphere-ionosphere dynamics. Thermospheric neutral winds, mostly below 250 km altitude, have been observed by Fabry-Pérot interferometers during the night and derived from incoherent scatter radar measurements for decades, but only at a few stations. Remote and in situ measurements of neutral winds also exist, covering various altitudes, mostly below 400 km, but only for a limited period. For example, ESA's GOCE is one of the largest collections of in-situ measurements in the 300–250 km altitude range, but it only covers the period 2009–2012 and local times of dawn and dusk. And cross-track neutral winds derived from CHAMP accelerometer data, covering all local times and the altitude range 455–320 km over the period 2001–2009. Characterising the winds, for example in terms of latitudinal, diurnal, seasonal and solar cycle variations, is a difficult task with these limited data. The literature also generally suggests that there are inconsistencies between these data products, not only by the technique used to derive the winds, but also by the station. Not surprisingly, the complex interrelationship of neutral winds in the dynamics of the upper atmosphere is not fully understood. A neutral wind product from the Swarm satellites will therefore be invaluable to the scientific community in resolving some of the difficulties in understanding thermosphere-ionosphere dynamics. With over 7 years of data (and counting), Swarm can provide a unique data product to characterise the neutral winds at all local times in its different orbital heights.

3.2 Approach

In the ionosphere-thermosphere region, collisional momentum exchange between plasma and neutrals is important, so that these hydromagnetic coupling processes affect the tidal winds. Thus, the conservation of momentum in this region is dominated by electromagnetic terms [RD-1]. The steady-state conservation of momentum for the i^{th} ionised species is,

$$\mathbf{0} = -\nabla P_i + \rho_i \mathbf{g} + N_i q_i (\mathbf{E} + \mathbf{V}_i \times \mathbf{B}) - \rho_i \nu_{in} (\mathbf{V}_i - \mathbf{U}), \quad (1)$$

where ∇P_i is the ion pressure gradient, ρ_i is the ion mass density, \mathbf{g} is the gravitational acceleration, N_i is the number density, q_i is the charge, \mathbf{E} is the electric field, \mathbf{V}_i is the ion velocity, \mathbf{B} is the magnetic field, ν_{in} is the collision frequency of ions with neutrals, and \mathbf{U} is the velocity of the neutral gas. The Lorentz force relates the effects of ion-neutral collisions on the neutrals. The simplified horizontal component of the Lorentz force is given by,

$$(\mathbf{J} \times \mathbf{B}) / \rho = -\epsilon_x (\mathbf{U} - \mathbf{V}_i) + \epsilon_y \cos(\theta) (\mathbf{U} - \mathbf{V}_i), \quad (2)$$

where \mathbf{J} is the current density, ρ is the neutral mass density, θ is the colatitude, \mathbf{V}_i is the mean ion drift velocity, and ϵ_x and ϵ_y are the Pedersen and Hall ion drag coefficients (Lorentz terms), respectively. The equation of motion of the neutral atmosphere must also account for the part of the neutral velocity controlled by nonelectrical forces, such as the Coriolis force and the neutral pressure gradient. Ignoring the second-order terms, we simplify the horizontal momentum equation for neutral zonal (u ; east-west) and meridional (v ; north-south) winds as follows,

$$\frac{\partial u}{\partial t} = A_u + B_u + C_u, \quad (3)$$

$$\frac{\partial v}{\partial t} = A_v + B_v + C_v. \quad (4)$$

A_u and A_v are the Coriolis force:

$$A_u = (2\Omega \sin \phi)v; \quad A_v = -(2\Omega \sin \phi)u, \text{ where } \Omega \text{ is the Earth's angular rotation rate.}$$

B_u and B_v are the ion drag force:

$$B_u = (\epsilon_x(u_e - u) + \epsilon_y(v_e - v)); \quad B_v = (\epsilon_x(v_e - v) - \epsilon_y(u_e - u)), \text{ where subscript e refers to the respective component in ion drift velocity.}$$

C_u and C_v are the pressure gradient force:

$$C_u = -\frac{1}{R_E \cos \phi} \frac{\partial P}{\partial \lambda}; \quad C_v = -\frac{1}{R_E} \frac{\partial P}{\partial \phi}, \text{ where } R_E \text{ is the radius of the earth and } \lambda \text{ is the longitude.}$$

The second order terms ignored here include curvature momentum force, turbulent flux divergence (horizontal and vertical diffusion), and nonlinear horizontal and vertical advection terms.

3.2.1 Lorentz terms

Assuming the masses of ions and neutrals are equal, ϵ_x and ϵ_y in Equations (3) and (4) are approximated as,

$$\epsilon_x \approx \frac{N_i}{N} \frac{\nu_{in}}{1 + (\nu_{in}/\omega_i)^2}; \quad \epsilon_y \approx \frac{\nu_{in}}{\omega_i} \epsilon_x,$$

where N_i is the ion number density, N is the neutral number density, and ω_i is the ion gyrofrequency.

We use the low rate magnetic field intensity data (level 1b product; < SW_OPER_MAGA_LR_1B>) from Swarm-A to calculate the gyrofrequency of O^+ ions as, $\omega_{O^+} = (e * B * N_A) / \bar{m}_O$, where e is the electron charge, N_A is the Avogadro constant, and \bar{m}_O is molecular mass of atomic oxygen.

In this feasibility study, we consider the collision frequencies of O^+ ions with atomic and molecular oxygen and molecular nitrogen. These compositions are determined through data assimilation with the NRLMSISE-00 model [RD-2]. Appendix A shows the calculated Lorentz terms.

3.2.2 Pressure gradient

We derive the pressure from the ideal gas law. Here the neutral mass density is directly substituted from the Swarm-A precise orbit determination data product (DNSAPOD ESA v.0201). The neutral temperature is obtained by data assimilation, where the NRLMSISE-00 model is calibrated against Swarm-A data [RD-2]. The outputs of the pressure gradients calculated in this way are shown in Appendix B.

3.2.3 Ion drift velocity

In this feasibility study, we experiment with substituting the ion drift velocities in Equations (3) and (4) with Swarm-A horizontal cross-track ion drift data (SW_EXPT_EFIA_TCT02; v.0302). The cross-track ion drift data are given in the satellite body frame, and thus before the substitution we rotate the wind vectors to the local north-east-down reference frame.

3.3 Study Periods

We select the following two time periods for the feasibility study:

1. 10–14 March 2015
2. 19–23 September 2020

Geomagnetic activity is generally low during these two periods. Solar activity is moderately high in 2015 and low in 2020. The space weather conditions during the two study periods are shown in Figures 2 and 3.

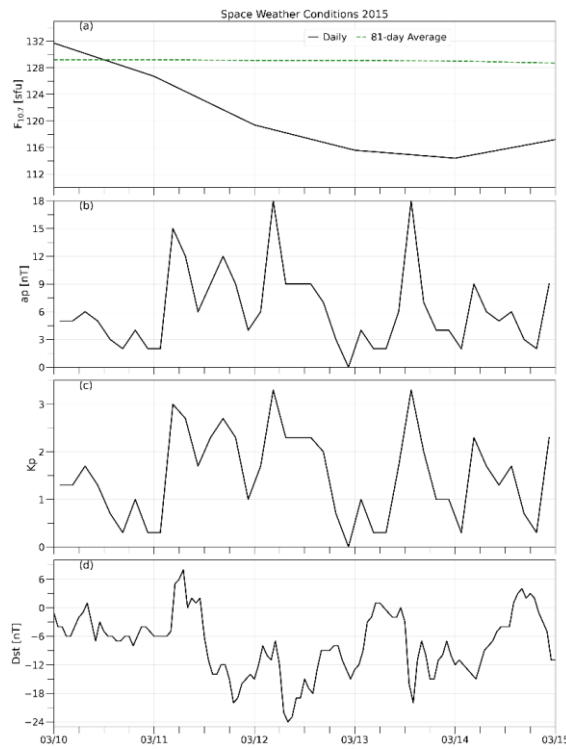


Figure 2: Space weather 10–14 March 2015 shown via Dst, Kp, 3-hour ap, and $F_{10.7}$.
 $1 \text{ sfu} = 10^{-22} \cdot \text{W} \cdot \text{m}^{-2} \cdot \text{Hz}^{-1}$.

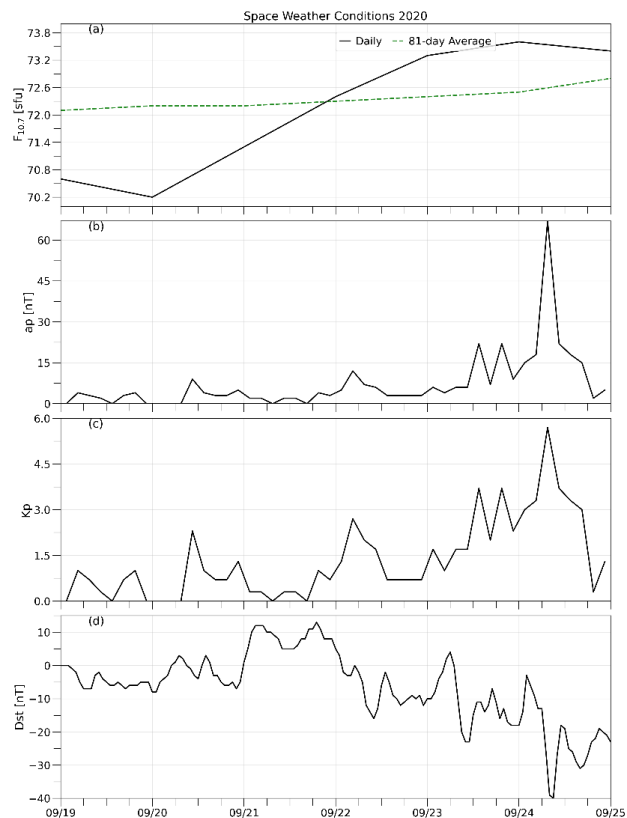


Figure 3: Same as Figure 2 except for 19–24 September 2020.

4 Swarm-A-derived neutral horizontal winds

Figure 4 shows the probability density distributions of Swarm-A-derived (top 4 panels) zonal and (bottom 4 panels) meridional wind velocities for the 2015 study period. In Figure 4 and in subsequent comparisons, we use the astropy's (astropy.org) convolution algorithm with a Gaussian filter to smooth out large unphysical values of the Swarm-A-derived winds (Appendix C). The results are compared with three commonly used models: TIE-GCM (thermosphere ionosphere electrodynamics general circulation model), and HWM (horizontal wind model) 2007 and 2014 versions.

Swarm-A-derived zonal winds do not show the bimodal structure shared by the models in Figure 4. Although Swarm-A median wind speed is similar to HWM-2014, Swarm-A has the largest standard deviation. Swarm-A-derived meridional winds show a slightly better agreement with the TIE-GCM distribution.

Similarly, Figure 5 also shows large data-model discrepancies in zonal winds compared to meridional winds for the 2020 study period. These probability density distributions indicate that the inherent structure of the Swarm-A winds is different from that of the models, except for a few statistical similarities.

In Figure 6, we present a statistical summary of the scalar horizontal wind speeds for the two study periods. Figure 6 shows that there is no linear correlation between Swarm-A and the models. The wind speed scale in Figure 6 is limited to 400 m/s for visualisation purposes. The number of data points above 400 m/s is not significant (not shown). Although the data are mostly distributed in the low wind speeds, Figure 6 reveals that the occurrence of high wind speeds in Swarm-A (e.g., above 200 m/s) is not random. The comparisons with TIE-GCM and HWM-2007 for 2015 show that Swarm-A underestimates where model wind speeds are large. Interestingly, HWM-2014 has the lowest standard deviation and generally does not produce winds below approximately 30 m/s, which appears to be systematic.

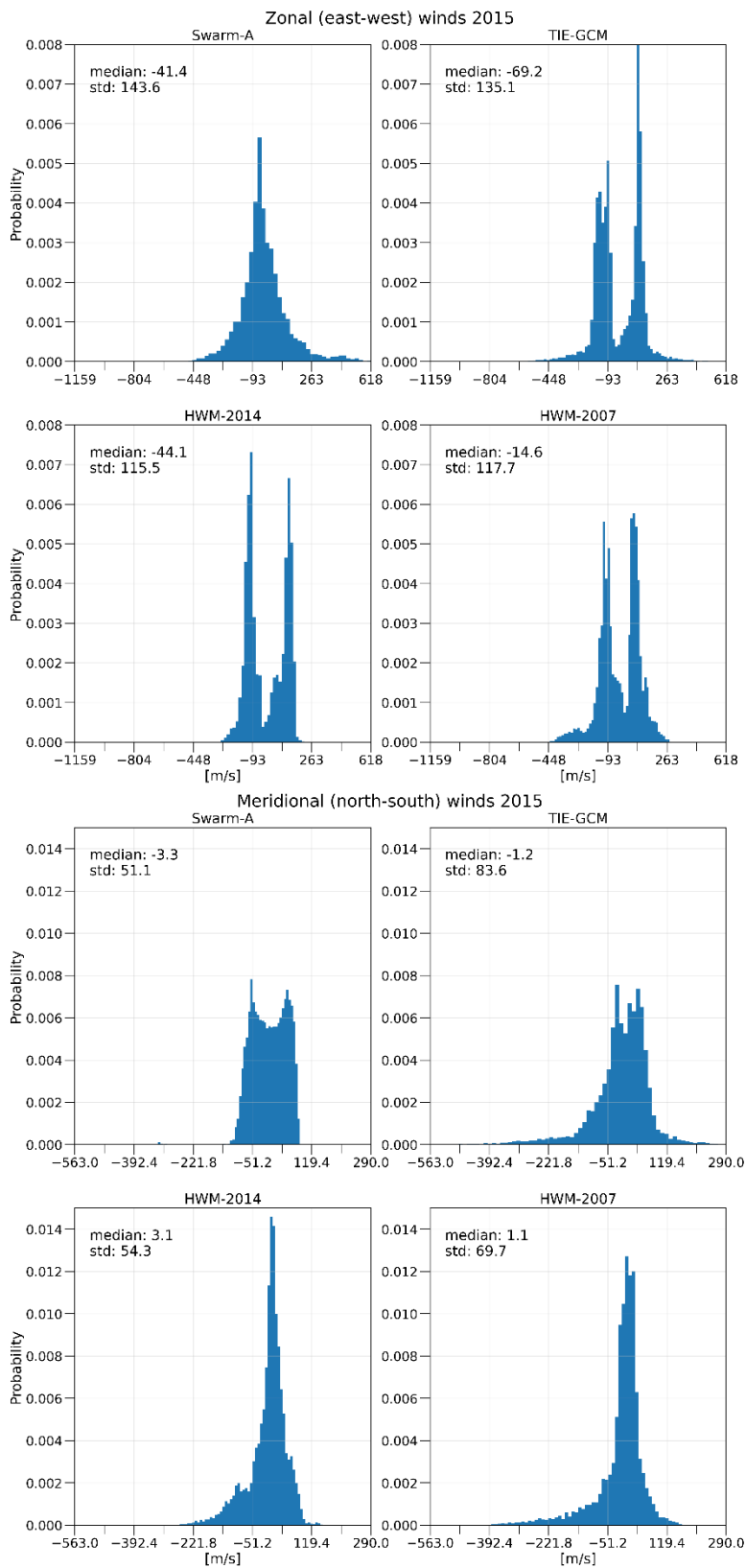


Figure 4: Probability density distributions of zonal and meridional winds—2015 study period.

The winds derived from Swarm-A are compared with the estimates from TIE-GCM, HWM-2007, and HWM-2014. Each panel also shows the median and standard deviation of each distribution. Positive zonal (meridional) winds are eastward (northward).

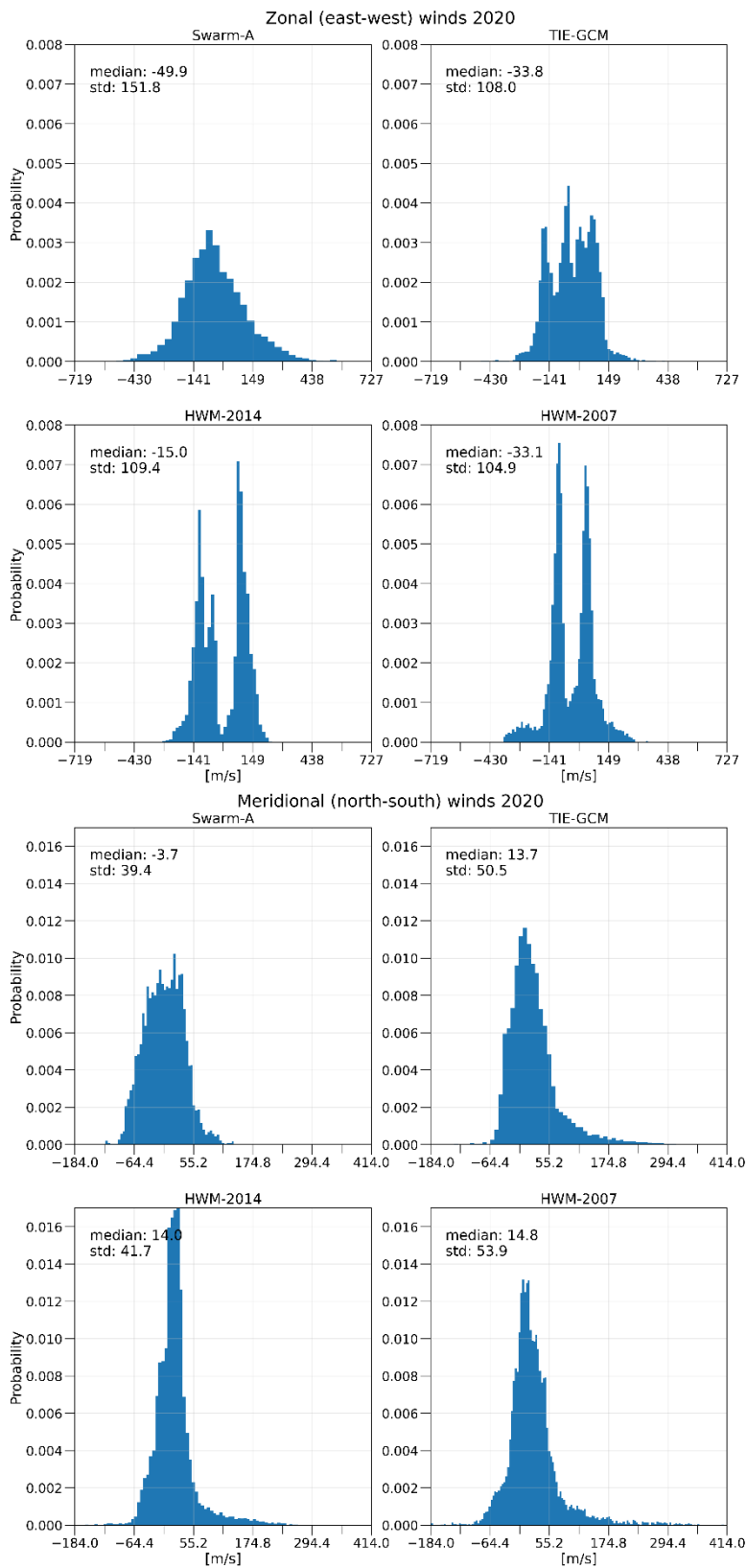


Figure 5: Same as Figure 4 except for the 2020 study period.

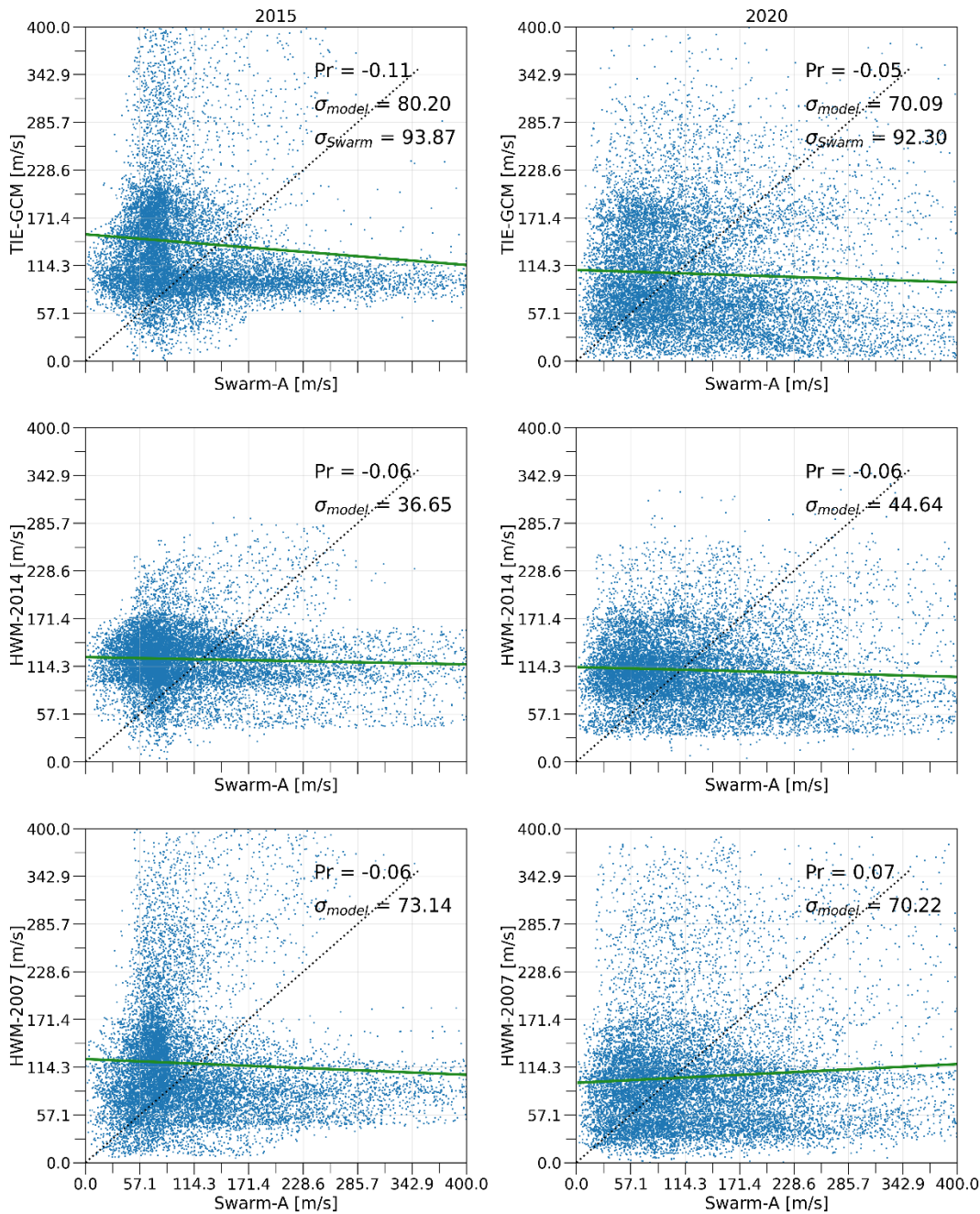


Figure 6: Statistical summary of the scalar horizontal wind speeds.

(left) 2015 and (right) 2020 study periods. Pr is the Pearson correlation coefficient between the abscissa and ordinate distributions. Standard deviations of the Swarm-A-derived winds and the models are given in units of m/s. The green solid line is a linear fit, and the black dotted line represents the ideal data-model reference.

4.1 Comparison of the latitudinal wind patterns

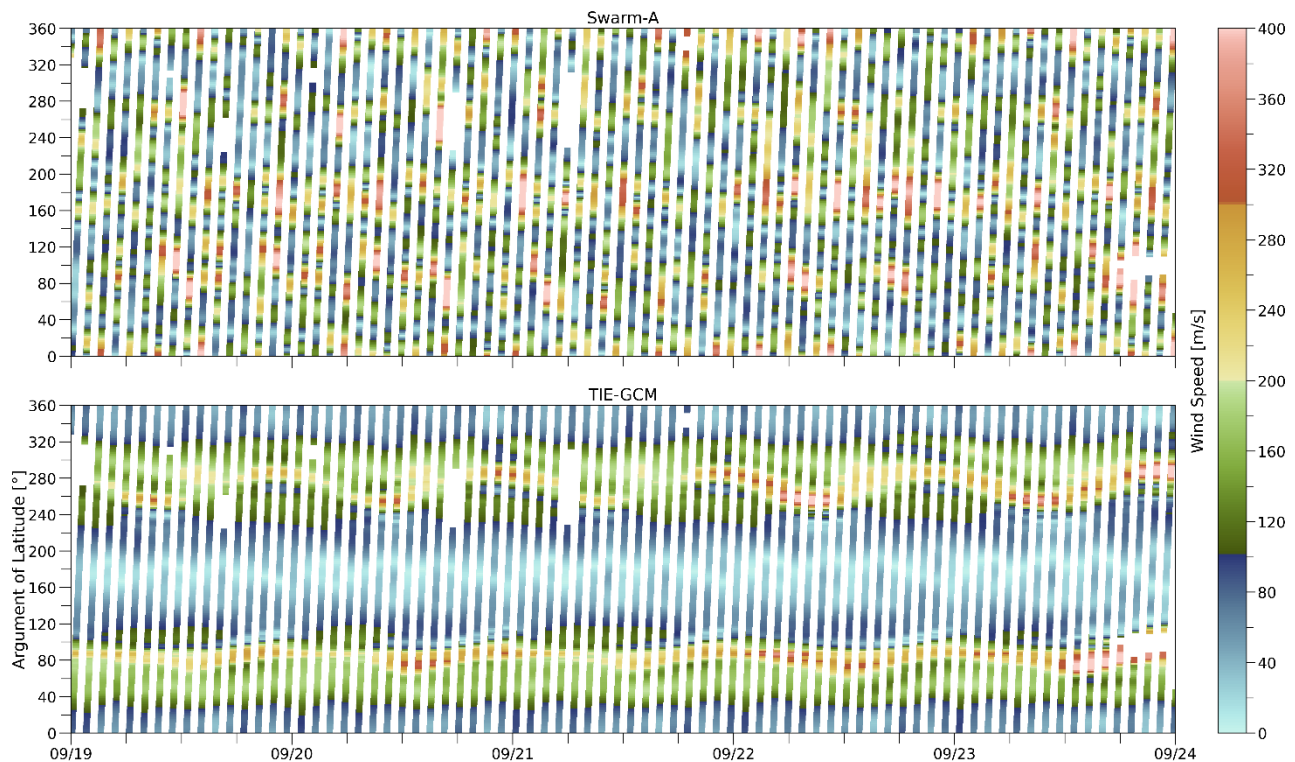


Figure 7: Swarm-A-derived winds compared with TIE-GCM for the 2020 study period.

Figure 7 examines the latitudinal patterns in the Swarm-A derived winds. Here we compare the Swarm-A results with the expected dynamics in theoretical winds. Figure 7 shows that in Swarm-A, high wind speeds occur consistently in both equatorial and high latitude regions, while low wind speeds (blue regions) are more common in mid-latitudes. The theoretical winds in TIE-GCM show that low wind speeds are expected near the equator.

Figures 8 and 9 compare the latitudinal patterns of the difference between Swarm-A-derived winds and model estimates. In both figures, the data-model agreement is better in the mid-latitudes compared to the equatorial and high latitudes.

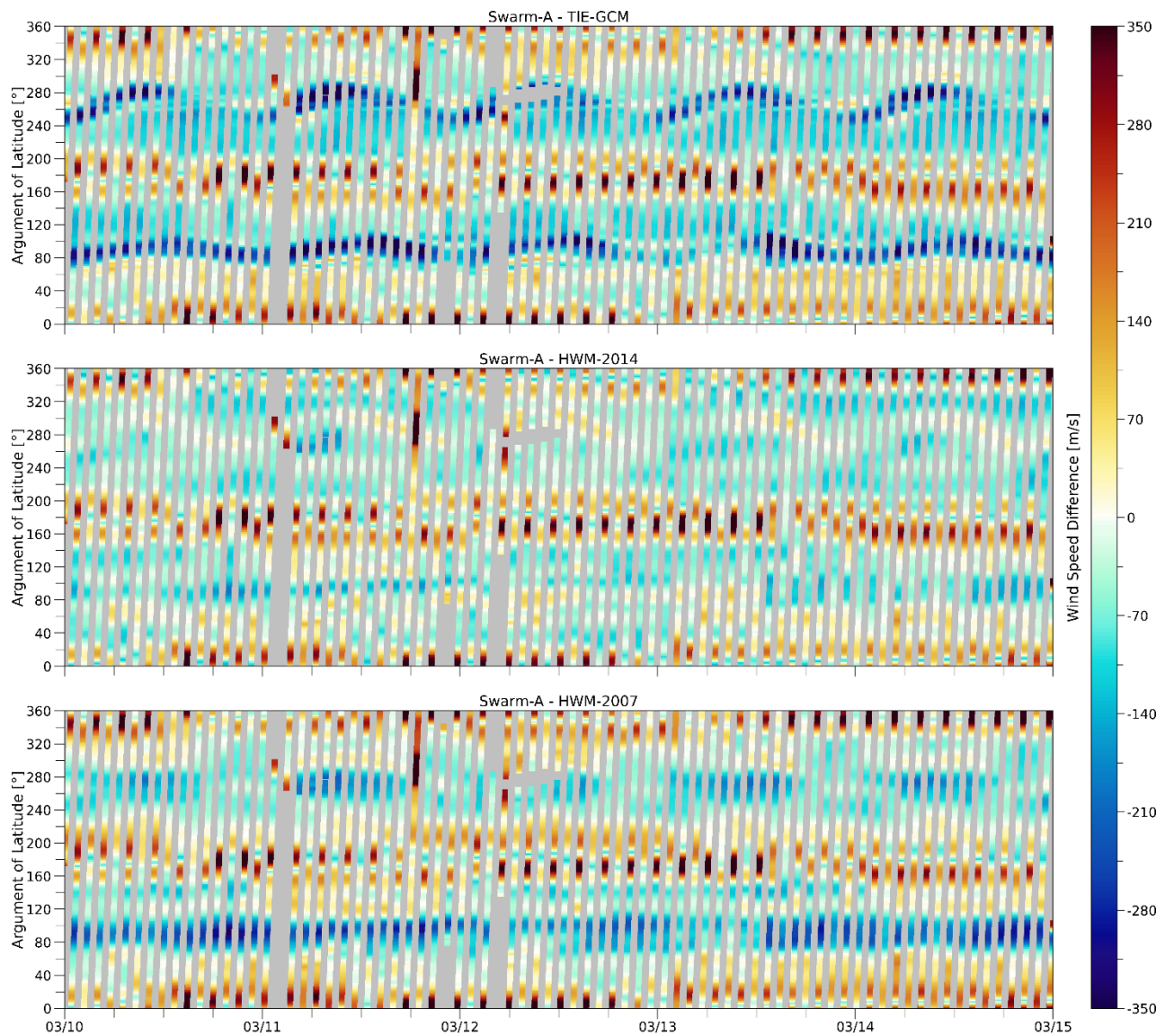


Figure 8: Data-model differences of the scalar horizontal wind speeds.

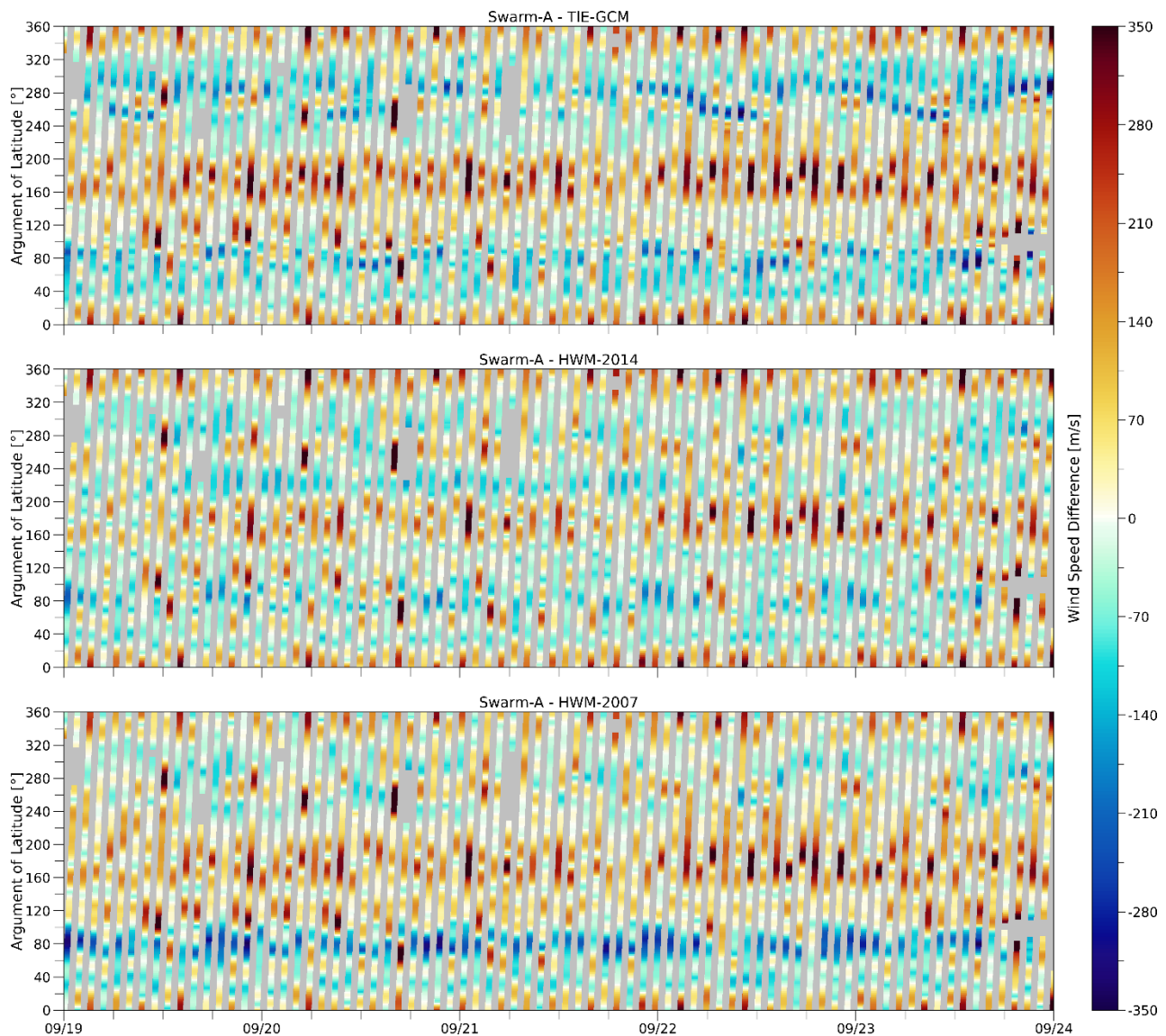


Figure 9: Same as Figure 8 except for the 2020 study period

4.2 Contribution from ion drift velocity

In order to compare the contribution of ion drift velocity, we perform two runs: one for the entire study period without Swarm-A cross-track ion drift velocities, and a second run for those cases where Swarm-A cross-track ion drift data are available. We smooth the two runs separately as described above. The difference between these two runs is shown in Figure 10. Some of the small differences in Figure 10 are due to the smoothing differences. From Figure 10 it can be concluded that the contribution of the ion drift velocities to reducing the large bias in the Swarm-A derived winds is minimal.

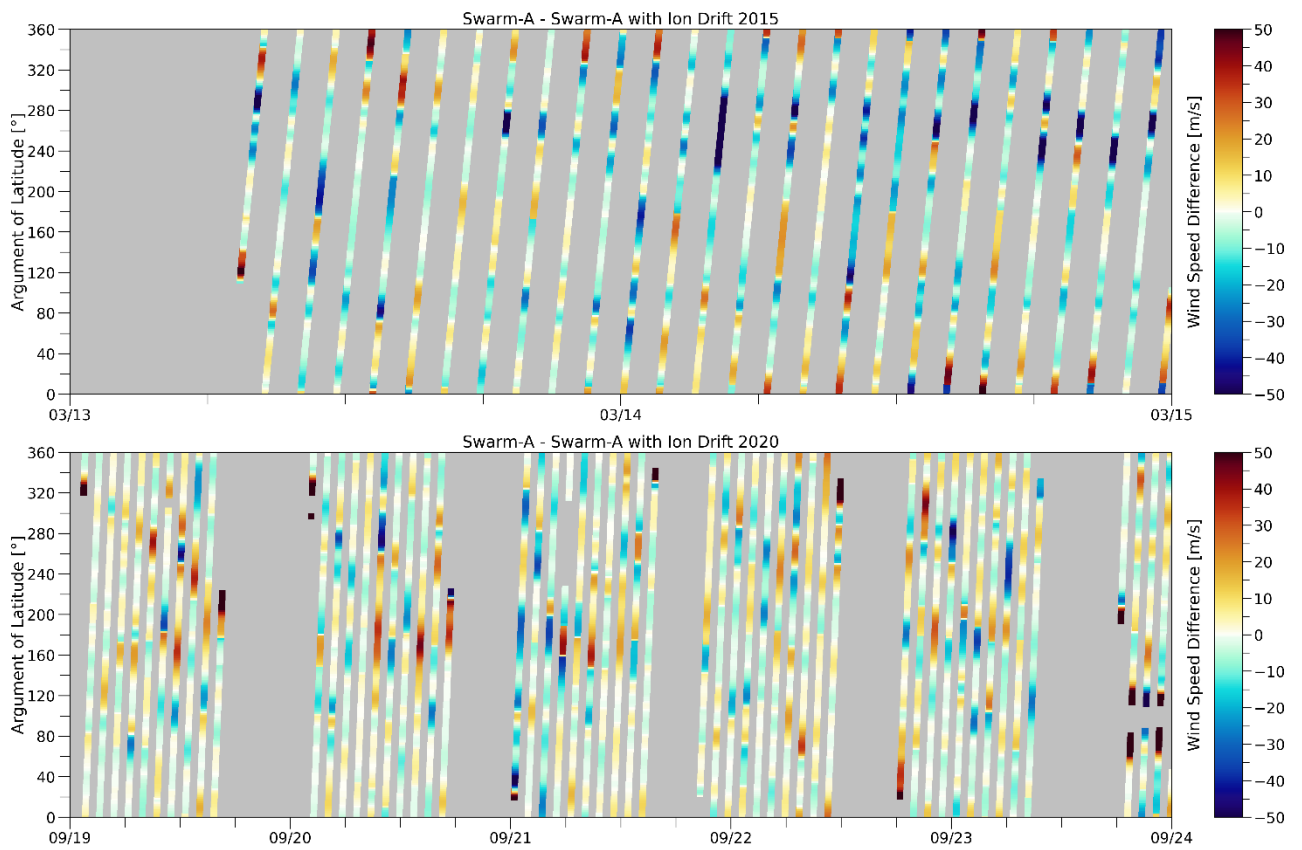


Figure 10: The difference between winds derived with and without ion drift velocities.

5 Summary and Conclusions

In this feasibility study, we solve for the horizontal wind fields along the Swarm-A orbit. While various in-situ measurements along the satellite's orbit could be used in the simplified horizontal momentum equation to solve for the winds, the results show a nonrandom large bias in the Swarm-A-derived winds compared to both physical and empirical models. The results of this study were presented at the AGU Fall Meeting 2022 [RD-3]. The study showed that deriving reliable wind fields from Swarm inputs is challenging and identifying the sources of uncertainty is complicated.

We also show that the Swarm-A winds derived as such lack certain latitudinal characteristics (e.g., Figure 7). The sources contributing to these latitudinal discrepancies remains to be identified. One suspect is the resulting relatively small pressure gradient force (see Appendix B). The Lorentz terms we computed from the Swarm data appear to be physically reasonable (see Appendix A). The neutral mass density gradient between the Swarm-A and -C orbital separations could be used to derive the pressure gradient. Such an experiment will be useful to validate the pressure gradients derived in this feasibility study. Furthermore, averaging over several months of data to construct statistically meaningful latitude-longitude bins could also help to resolve pressure gradients and subsequently neutral winds.

Swarm also provides current density data, the use of which in the $\mathbf{J} \times \mathbf{B}$ term of Equation (2) should be further investigated. In order to develop a reliable wind product from Swarm data, a thorough validation procedure should be followed at various stages of data processing, including the determination of input parameters such as pressure gradients. While data assimilation with physics-based models may not be ideal for continuous processing of Swarm wind outputs, some targeted data assimilation studies could help to capture some of the important nonlinear terms relating Swarm input data to neutral winds.

A Lorentz terms

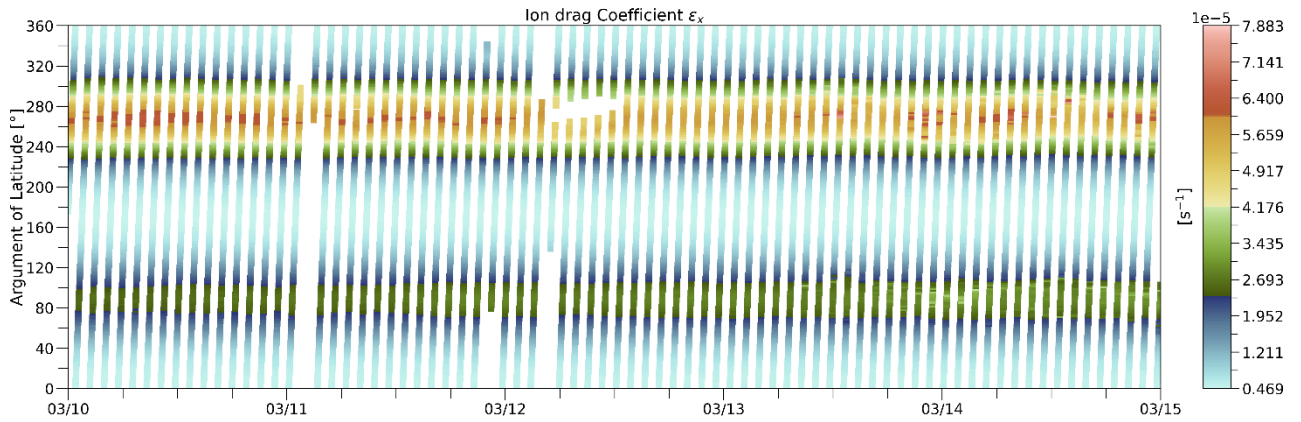


Figure 11: The Pedersen ion drag coefficient ϵ_x for the 2015 study period.

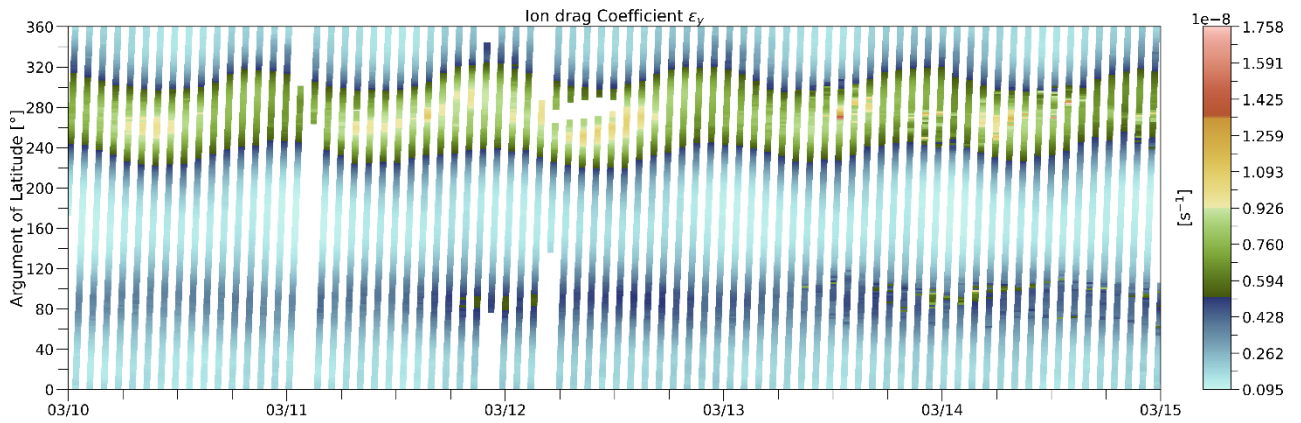


Figure 12: Same as Figure 11 except for Hall ion drag coefficient ϵ_y .

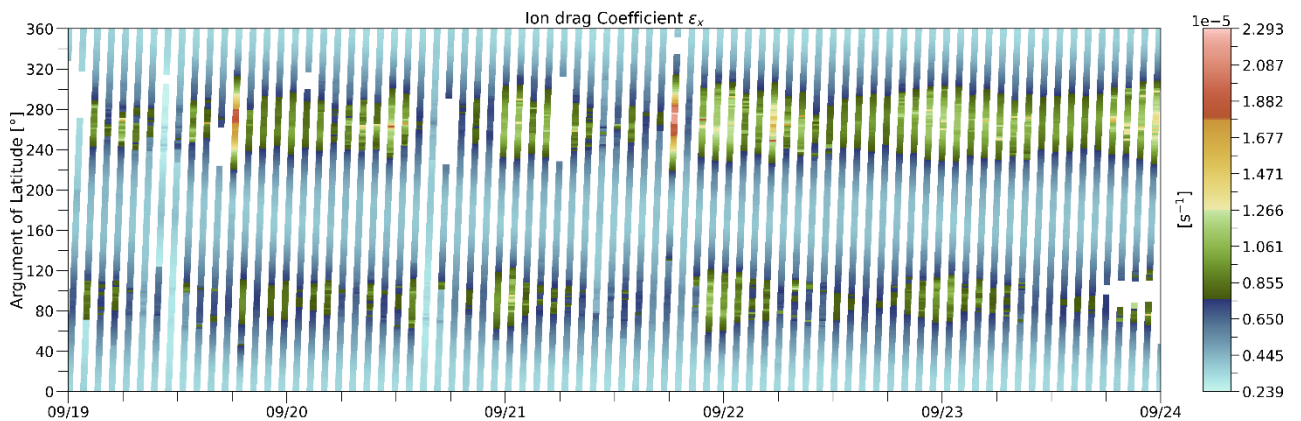


Figure 13: Same as Figure 11 except for the 2020 study period.

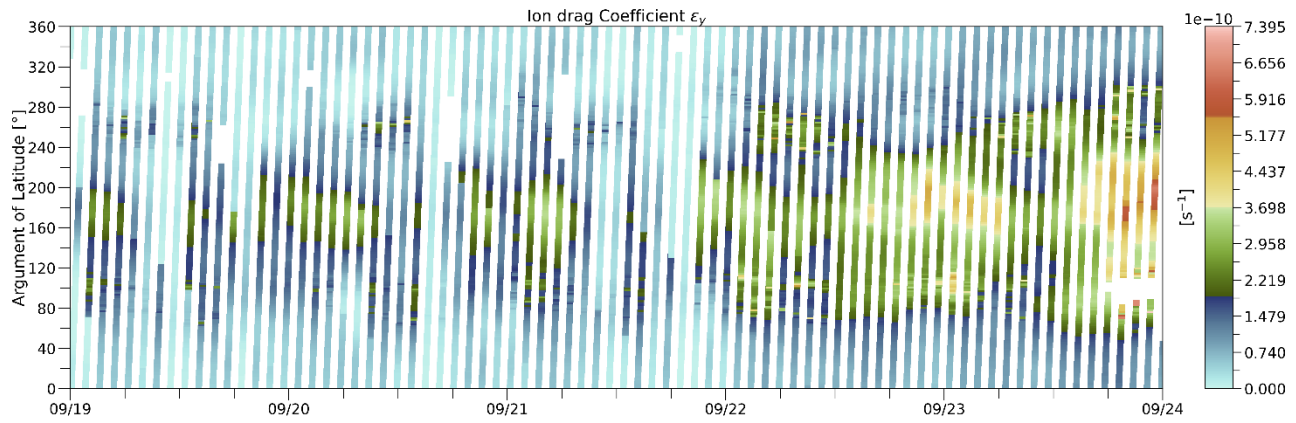


Figure 14: Same as Figure 12 except for the 2020 study period.

B Pressure gradients

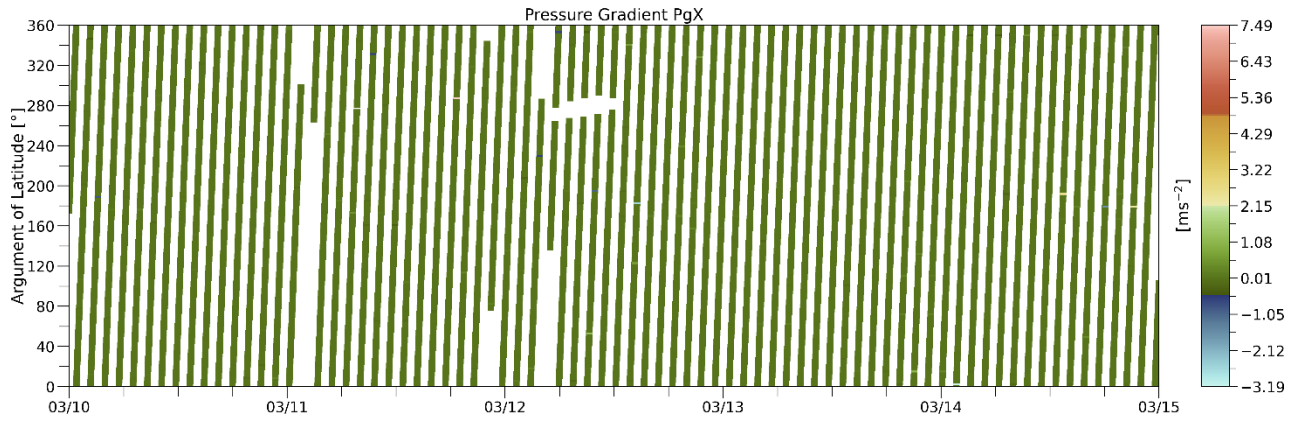


Figure 15: Pressure gradient PgX with respect to longitude—2015 study period.

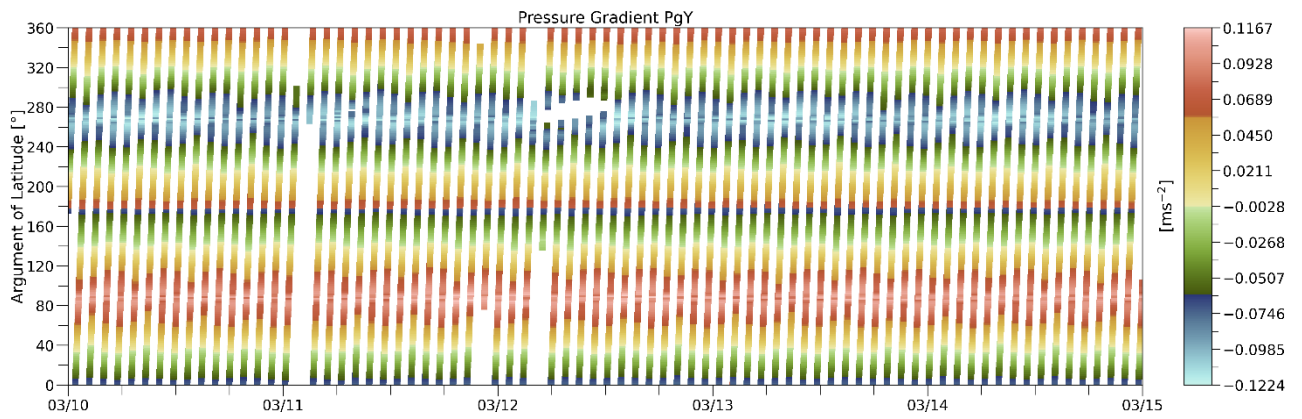


Figure 16: Pressure gradient PgY with respect to latitude—2015 study period.



Figure 17: Same as Figure 15 except for the 2020 study period.

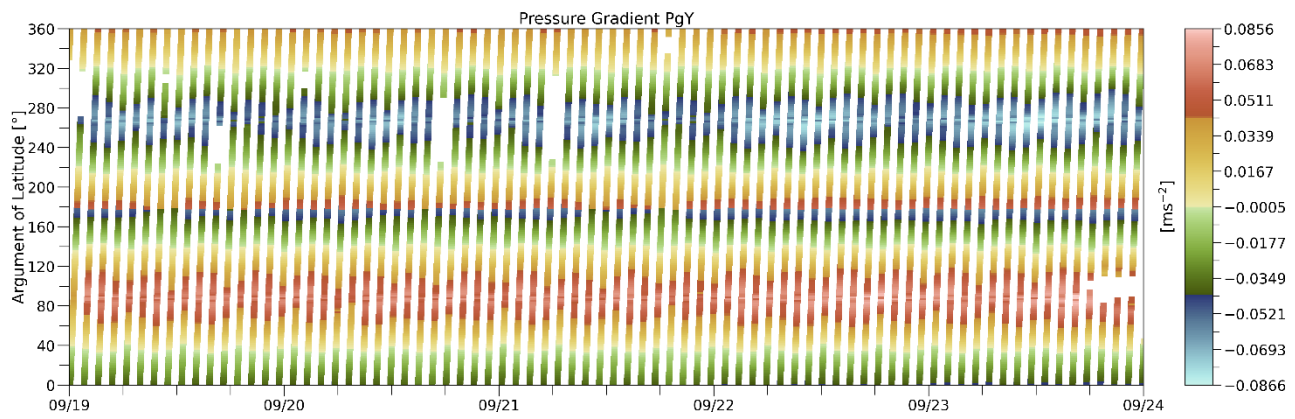


Figure 18: Same as Figure 16 except for the 2020 study period.

C Nonsmoothed winds

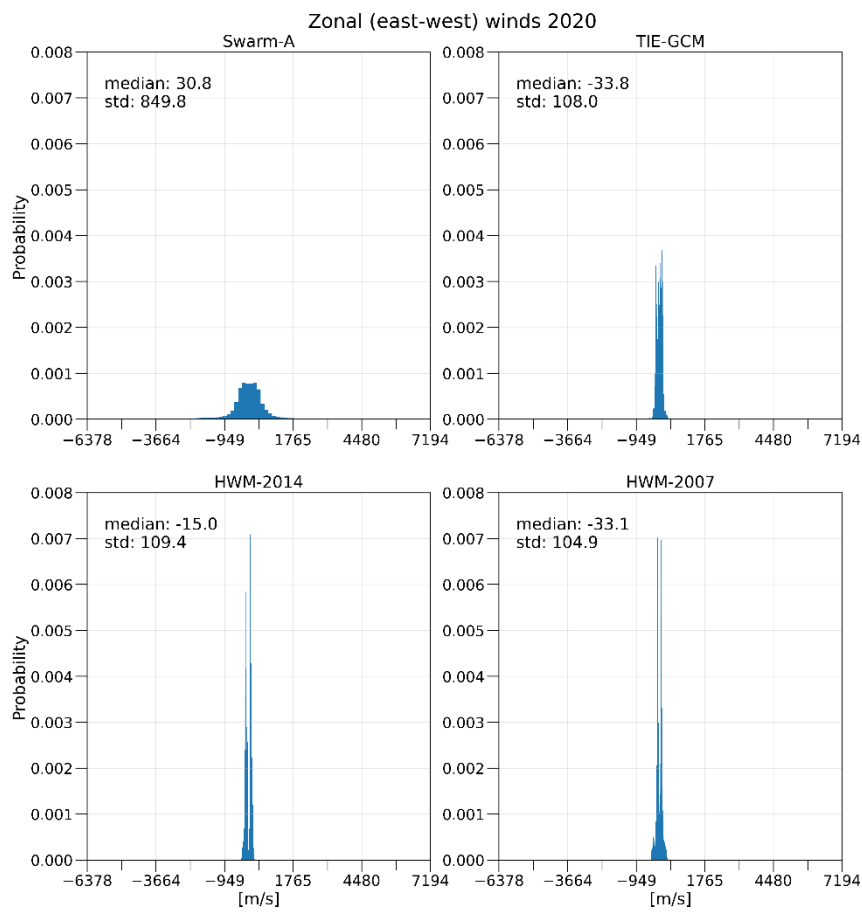


Figure 19: Similar to Figure 5 except for nonsmoothed Swarm-A.